Self-assembly of amphiphilic copolymers containing polysaccharide: PISA versus nanoprecipitation, and the temperature effect

Djallal Ikkene, Ana Andreea Arteni, Malika Ouldali, Jean-Luc Six, Khalid Ferji

Self-assembly of Amphiphilic Copolymers Containing Polysaccharide: PISA versus Nanoprecipitation, and the Temperature Effect.

Djallal Ikkene,[a] Ana Andreea Arteni,[b] Malika Ouldali,[b] Jean-Luc Six[a] and Khalid Ferji*[a]

"This manuscript is a tribute to the 50 year anniversary of the French Polymer Group (Groupe Français des Polymères - GFP)"

For many decades, the self-assembly of amphiphilic copolymers containing polysaccharide, called glycopolymers, has been induced in water *via* nanoprecipitation, whereas the polymerization-induced self-assembly (PISA) approach has been less reported. Using advanced characterization techniques including static/dynamic light scattering and TEM/CryoEM analyses, we studied the impact of the experimental conditions/process on the morphology of formed glyco-nanostructures. A model amphiphilic glycopolymer (Dex-g^{12}-PHPMA$_{400}$) based on dextran as hydrophilic polysaccharide backbone and poly(2-hydroxypropyl methacrylate) (PHPMA) as hydrophobic grafts were prepared in water using a photo-induced RAFT polymerization at 405 nm. On the one hand, our findings revealed that photo-initiated PISA (photo-PISA) at room temperature (RT) led to a mixture of spheres with a significant population of worm-like micelles (WLM), whereas the nanoprecipitation of purified Dex-g^{12}-PHPMA$_{400}$ led only to spherical micelles. On the other hand, we demonstrate that the morphology of the produced glyco-nanostructures is affected by temperature since performing photo-PISA at 60°C led to spheres instead of WLM. Finally, our findings revealed that pre-synthesized WLM at RT underwent irreversibly an unusual morphological transition to spheres by heating to 60°C.

Introduction

Amphiphilic copolymers containing natural hydrophilic polysaccharides and hydrophobic synthetic polymers, called amphiphilic glycopolymers (AGPs), are promising materials for cosmetic, food and biomedical applications. [1-6] For many decades, the self-assembly of AGPs in water has been induced *via* "conventional assembly processes", [6, 7] including nanoprecipitation,[8-14] and emulsion-solvent evaporation. [15-22] Namely, in these pathways, pre-synthesized amphiphilic copolymers are initially dissolved in a common organic solvent for both blocks followed by a gradual addition of water, a selective solvent for one of the blocks, to induce the formation of nanoobjects. Although such processes are relatively simple to perform at the laboratory scale, their industrial transposition is limited due to the low solids concentration (typically <1 %wt) prepared and the multiple processing and purification steps required. Moreover, performing these traditional processes with AGPs frequently leads to the formation of kinetically-trapped aggregates, while advanced morphologies (worm-like micelles and vesicles) are rarely reached, due to the difficulty to find a common organic solvent of AGPs.[6, 23, 24]

Polymerization-induced self-assembly (PISA)[25-27] is a straightforward and efficient approach recently developed to formulate polymeric nanostructures with diverse morphologies in both polar and apolar solvents. [28-40] Compared to the conventional assembly processes, PISA is a one-pot approach requiring simple operating conditions to produce nanoobjects at high solids concentration (up to 50 wt%),[41-43] without recourse to any additional purification steps. PISA involves a chain-extension of a solvophilic macromolecular stabilizer with a desired monomer that forms a solvophobic block when reaching a critical chain-length. This results in a spontaneous self-assembly of the produced amphiphilic copolymer into nanostructures of various sizes and morphologies depending on the relative volume ratio of each blocks and on the solids concentration. Although nitroxide mediated polymerization (NMP) [25, 41] was the first reversible-deactivation radical polymerization (RDRP) technique carried out in PISA, reversible-addition fragmentation chain transfer (RAFT) polymerization [44-58] is by far the most reported one in the literature. Currently, the scope of PISA has been extended to many other polymerization mechanisms.[59-71]

Since its discovery, aqueous PISA has been intensively conducted using hydrophilic synthetic macromolecular precursor as reactive stabilizer, including poly(ethylene oxide), poly(glycerol monomethacrylate), and poly((meth)-acrylic acid) whereas natural polysaccharides have been scarcely reported. [6] Bernard *et al*. [72] prepared submicronic latex particles *via* aqueous RAFT polymerization of vinyl acetate from a xanthate-terminated dextran at 65°C. Kapishon *et al*. [73] prepared spherical micelles by polymerizing methyl methacrylate (MMA) from alginate-based macroinitiator using single electron transfer living-radical polymerization (SET-LRP). Hatton *et al*.[74] described the synthesis of spherical latex particles by carrying out RAFT-mediated surfactant-free emulsion polymerization to chain-extend MMA from xyloglucan-based macromolecular chain transfer agent. Surprisingly, only low-order morphology

(spheres) was observed in these works, even when different AGPs compositions were targeted. We guess this is due to the temperature (> 60 °C) used to thermally produce radicals required for the chain-extension of the core-forming hydrophobic block.

Over the last few years, light has emerged as a promising alternative initiation pathway to mediate RDRPs (photo-RDRP) at room temperature (RT). [40, 75-79] Among the different reported strategies,[80-84] photo-mediated RAFT polymerization (photo-RAFT) [85, 86] was quickly distinguished as the technique of choice to drive aqueous PISA at RT (photo-PISA),[49, 57, 58, 87-89] due to its ability to control the polymerization of a wide range of monomers (notably thermoresponsive ones [90, 91]) at mild temperature conditions. Currently, the activation of the photo-RAFT using an exogenous photoinitiator, [58, 88, 91-93] is the most commonly strategy applied in photo-PISA. Other mechanisms using the direct photodissociation of a RAFT agent (iniferter) under UV irradiations, [49] visible light, [89, 94] or by photo electron transfer RAFT (PET-RAFT)[95, 96] in the presence of a photocatalyst have been also reported.[57, 97]

Recently, our group reported the first example of advanced morphologies based on a natural polysaccharide stabilizer (dextran) using the features of photo-PISA at RT. [49] A functionalized dextran with RAFT agents ($DexCTA_{12}$) was chain extended in water by 2-hydroxypropyl methacrylate (HPMA) using photo-RAFT polymerization under 365 nm irradiations at RT.

Herein, we continue our series of investigations aiming to understand the parameters influencing the self-assembly of AGPs in water, by studying the impact of the self-assembly methods and the temperature on the morphology of the resulted nanoobjects. On the one hand, for an identical chemical composition of the AGP (Dex-g^{12}-$PHPMA_{400}$ containing on average 12 PHPMA grafts per dextran chain, $\overline{X_n}$ of each graft = 400), we investigated the nanoobject morphologies generated by the photo-PISA approach and the conventional assembly processes. More precisely, Dex-g^{12}-$PHPMA_{400}$ -based nanoobjects were prepared *via* photo-RAFT PISA of HPMA from $DexCTA_{12}$ in water at RT (Fig. 1). The Dex-g^{12}-$PHPMA_{400}$ glycopolymer was then recovered by freeze-drying the PISA suspension, and dispersed in water to prepare glycopolymers-based nanostructures (glyco-nanostructures) *via* nanoprecipitation, emulsion-solvent evaporation, and film rehydration methods using usual organic solvents. On the other hand, the effect of temperature on the evolution of the nanostructures morphology was studied, both by heating the previous PISA suspension and by conducting the photo-PISA at 60 °C. A detailed physico-chemical investigation of the glyco-nanostructures, using light scattering and (cryo)transmission electron microscopy, shows that the morphologies strongly depend on the process and on the experimental conditions.

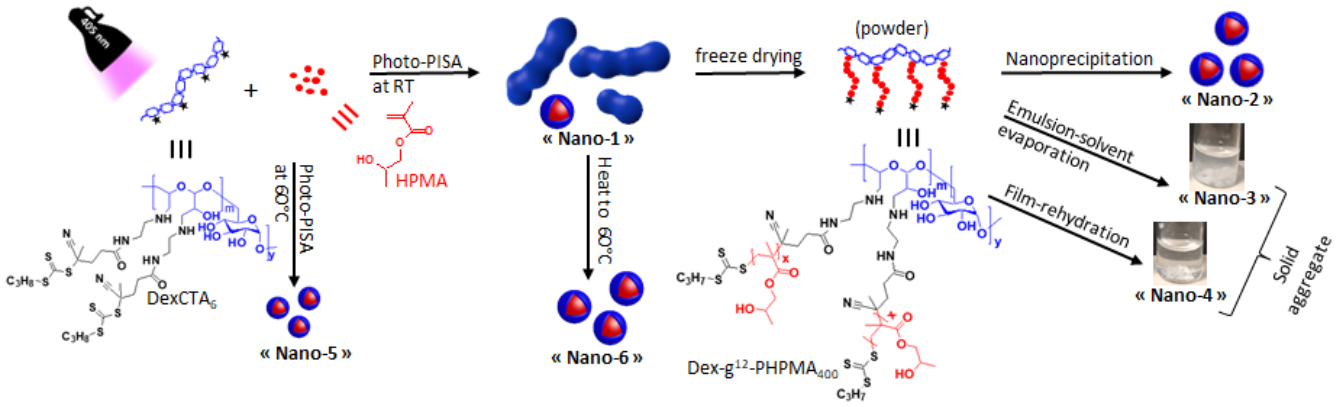

Fig. 1. Synthetic pathway of Dex-g^{12}-$PHPMA_{400}$-based nanostructures. Nano-1 was obtained by an aqueous photo-PISA of HPMA from $DexCTA_{12}$ at RT ($DexCTA_{12}$ contains 12 CTA groups per dextran chain). Nano-2, Nano-3, and Nano-4 were produced from dried Dex-g^{12}-$PHPMA_{400}$ using nanoprecipitation, emulsion-solvent evaporation and film-rehydration processes, respectively. Nano-5 was produced by an aqueous photo-PISA of HPMA from $DexCTA_{12}$ at 60 °C. Nano-6 was obtained by heating Nano-1 at 60 °C for 40 days.

Experimental.

Material.

Dextran T_{40} ($\overline{M_n}$ = 32000 g mol^{-1}, and Đ = 1.4), dimethyl sulfoxide (>99.9%), acetone, chloroform and dimethyl formamide were purchased from Merck. Ethyl (2, 4, 6-trimethylbenzoyl) phenylphosphinate (TPO-L) was purchased from fluorochem. 2-Hydroxypropyl methacrylate (HPMA) (98%) was purchased from ABCR and was passed through a silica column prior to use. ^{1}H NMR spectrum of HPMA (Fig. S1A†) revealed the presence of 25 mol % of the isomer (2-hydroxyisopropyl methacrylate, HIPMA). In the following, only the chemical structure of HPMA will be considered to simplify the chemical structures of polymers produced.

Synthesis of the macromolecular chain transfer agent, $DexCTA_{12}$.

The macromolecular chain transfer agent containing 12 CTA groups per dextran chain (Fig. S1B† and S2†) was prepared by modification of dextran using a multistep pathway as we previously reported.[11]

Nanoobjects formulation.

Nano-1 suspension was obtained *via* an *in-situ* aqueous photo-PISA of HPMA at RT. In a dried schlenk flask, $DexCTA_{12}$ (0.047 g, 0.0176 mmol of CTA groups) and HPMA (1 g, 6.95 mmol) were dissolved in

distilled water (9.5 mL) to reach *in fine* 10 % w/w solids. The reaction mixture was purged with nitrogen in the dark for 10 minutes. TOP-L (18 µL of TPO-L stock solution in DMSO at 100 mg mL^{-1}, 0.0057 mmol) was then added to the reaction medium under nitrogen. The mixture was then irradiated with a homemade UV–VIS LED (405 nm, 10 mW cm^{-2}) at RT for 1 hour to achieve full monomer conversion (Fig. S1C†), leading to the synthesis of Dex-g^{12}-$PHPMA_{400}$ glycopolymer. The experiment was carried out twice to verify the repeatability. This glycopolymer was freeze-dried overnight to recover a dried glycopolymer (powder), which was used to prepare Nano-2, Nano-3 and Nano-4 suspensions as described below.

Nano-2 suspension was prepared by nanoprecipitation. In a typical experiment, dried Dex-g^{12}-$PHPMA_{400}$ (20 mg) was solubilized in DMSO (1 mL), then added manually dropwise (200 µL min^{-1}) into distilled water (1 mL) under fast and regular stirring. Finally, DMSO was removed by dialysis against water for 3 days. The final concentration of this suspension was adjusted to 20 mg mL^{-1}.

Nano-3 suspension was prepared by emulsion-solvent evaporation. In a typical experiment, dried Dex-g^{12}-$PHPMA_{400}$ (20 mg) were solubilized by CH_2Cl_2 or $CHCl_3$ (1 mL) as water non-miscible organic solvent, then milli-Q water (2 mL) was added. An emulsion was obtained by sonication of the mixture for 30 min using a Vibracell 75 model (Bioblock Scientific, pulsed mode, 46 W). The organic solvent was evaporated during this sonication step.

Nano-4 suspension was prepared by film rehydration. In a typical experiment, dried Dex-g^{12}-$PHPMA_{400}$ (20 mg) was solubilized by 1 mL of acetone or THF as volatile organic solvent, followed by the slow evaporation of the solvent under reduced pressure to form a thin film, which was then rehydrated by milli-Q water under gentle stirring overnight.

Nano-5 suspension was obtained *via* an *in-situ* aqueous photo-PISA of HPMA at 60°C. In a dried schlenk flask, $DexCTA_{12}$ (0.047 g, 0.0176 mmol of CTA groups) and HPMA (1 g, 6.95 mmol) were dissolved in distilled water (9.5 mL) to produce 10 % w/w solids. The reaction mixture was purged with nitrogen in the dark for 10 minutes. The schlenk flask was immersed in a water bath heated to 60 ° C using a hot plate stirrer (IKA ™), before adding TPO-L (18µL of TPO-L stock solution in DMSO at 100 mg mL^{-1}, 0.0057 mmol) under nitrogen. Finally, the mixture was irradiated with a homemade UV–VIS LED (405 nm, 10 mW.cm^{-2}) for 1 h to achieve full monomer conversion (Fig. S1D†), leading to the synthesis of Dex-g^{12}-$PHPMA_{400}$ glycopolymer. The experiment was carried out twice to verify the repeatability.

Nano-6 suspension was obtained by incubating Nano-1 suspension (10 % w/w solids) at 60 °C using a thermoshaker (thermoshake THO 500/1 Gerhardt) for 40 days. The experiment was carried out twice to verify the repeatability.

^{1}H NMR spectroscopy.

All ^{1}H NMR spectra were acquired on a Bruker Avance 300 MHz, and carried out in DMSO-d_6.

Size exclusion chromatography (SEC).

A Shimadzu SEC device was equipped with a HPLC pump (LC 20AD, Shimadzu), degasser AF (DGU – 20A3R, Shimadzu), three PLgel columns (100000, 1000, and 100 Å), a Multi-Angle Laser Light Scattering (MALLS) detector (Mini Dawn Wyatt), a differential refractometer detector (RID 10A, Shimadzu), and an UV detector (SPD-20A, Shimadzu). The number-average molar mass ($\overline{M_n}$), weight-average molar mass ($\overline{M_w}$) and dispersity ($Đ$) were measured using DMSO/$NaNO_3$ (8.5 g L^{-1}) as eluant at flow rate of 0.7 mL min^{-1} at 70 °C. The refractive index increment (dn/dc = 0.025 mL g^{-1}) of Dex-g^{12}-$PHPMA_{400}$ glycopolymer was determined as previously reported. [11]

UV Absorbance.

UV-Visible absorbance spectra of thiocarbonate RAFT agent (CTA) in DMSO were recorded (Fig. S3†) using the UVikon-XL spectrometer (Bio-Tech instruments).

Dynamic/static light scattering (DLS/SLS).

Light-scattering measurements were performed using an ALV/CGS-3 compact goniometer system, equipped with an ALV-7004 multiple tau digital correlator and a vertically-polarized He-Ne laser of 22 mW output power operating at wavelength λ = 632.8 nm. During the analysis, the sample was kept in a toluene bath to keep the sample temperature constant (20 °C or 60°C) and to suppress reflections from the glass-air-interface of the sample cell. Scattered light was detected at scattering angles $20° \leq \theta \leq 150°$, corresponding to scattering vector regime $0.00459\ \mathrm{nm}^{-1} \leq q \leq 0.00255\ \mathrm{nm}^{-1}$. q is calculated using Eq-1, where n is the refractive index of the solvent (water).

$$q = \frac{4\pi n}{\lambda}\sin(\frac{\theta}{2}) \qquad \text{Eq-1}$$

In DLS, the autocorrelation functions were analysed in terms of relaxation time (τ) distribution according to the REPES routine. Z-average hydrodynamic radius (R_H) was estimated using the Stokes-Einstein equation (Eq-2), where D_0 is the diffusion coefficient of the nanoobjects determined from the slope of the q^2 dependence of relaxation rate ($\langle\Gamma\rangle = Dq^2$), k_B is the Boltzmann constant, T is the absolute temperature and ηs is the viscosity of the solvent (water). The polydispersity (PDI) was determined at θ = 90° using the second-order cumulant analysis.

$$R_H = \frac{k_B T}{6\pi\eta_s D_0} \qquad \text{Eq-2}$$

In SLS, the $\frac{Kc}{R_\theta}$ ratio is recorded in order to determine the radius of gyration (R_g) using the Zimm equation (Eq-3), where R_θ is the average scattered intensity measured at angle θ, K is an optical constant, c is the concentration of the nanostructure dispersion, A_2 is the second virial coefficient of the suspension and $\overline{M_w^{nano}}$ is the weight-average molar mass of the nanoobjects. K is calculated using equation (Eq-4), where N_A is Avogadro's constant, and $\frac{dn}{dc}$ is the refractive index increment of the nanostructure dispersion (dn/dc = 0.145 mL g^{-1}), measured in water using a differential refractometer Waters 410.

$$\frac{Kc}{R_\theta} = \frac{1}{\overline{M_w^{nano}}P(\theta)} + 2\mathrm{A}_2\mathrm{c} = \frac{1}{\overline{M_w^{nano}}}\left(1 + \frac{1}{3}R_g^2 q^{\,2}\right) + 2\mathrm{A}_2\mathrm{c} \qquad \text{Eq-3}$$

$$K = \frac{4\pi^2 n^2}{N_A\lambda^4}\left(\frac{dn}{dc}\right)^2 \qquad \text{Eq-4}$$

Eq-3 can be simplified for diluted systems (Eq-5) to determine the nanoparticle form factor P(θ) at each angle (θ). In practice, a

normalized form factor (Eq-6) is calculated relative to the form factor at θ = 20° to analyse SLS data.

$$P(\theta) = \frac{R_\theta}{Kc} \times \frac{1}{M_w^{nano}} \quad \text{Eq-5}$$

$$\text{Normalized form factor} = \frac{P(\theta)}{P(\theta=20°)} = \frac{\frac{Kc}{R(\theta=20°)}}{\frac{Kc}{R(\theta)}} \quad \text{Eq-6}$$

Transmission electron microscopy (TEM).

Samples were analysed by conventional electron microscopy using the negative staining method. 3 µL suspension (1 mg mL^{-1}) were deposited on an airglow-discharged carbon-coated grid. Excess liquid was blotted, and the grid rinsed with 2 % w/v aqueous uranyl acetate. The grids were visualised at 100 kV with a TECHNAI Spirit (FEI) transmission electron microscope (ThermoFisher, New York NY, USA) equipped with a K2 Base 4k x 4k camera (Gatan, Pleasanton CA, USA). Magnification was at 4400, 6500 or 15000 X, corresponding to a pixel size at the level of the specimen of 0.83, 0.55 and 0.25 nm, respectively.

Cryogenic electron microscopy (CryoEM).

CryoEM was performed using a Vitrobot Mark IV. 3 µL suspension (1 mg mL^{-1}) were deposited on airglow-discharged Quantifoil R2/2 grids. The sample was blotted for 3 seconds using force value 2, and frozen in liquid nitrogen-cooled ethane. Grids were observed on a FEI Tecnai 200, equipped with a field emission gun and operated at 200 kV. Images were recorded on a K2 Summit camera (Gatan) at a magnification of 15,000 at the level of the microscope (0.25 nm per pixel) and 1.5-3 microns defocus. Data were recorded under low-dose conditions (dose rate 20e/A2).

Results and discussion.

Photo-RAFT polymerization system.

In the present study, a thiocarbonate-type RAFT agent (CTA) was chosen to carry out the photo-PISA given its ability to initiate and control the polymerization of methacrylates under UV-vis irradiation.[94] The absorption of this CTA in UV region (~ 320 nm, π → π* electronic transition) and in visible region (~430 nm n → π*) (Fig S3A†) results in the generation of a carbon radical, which can initiate and control the chain propagation either *via* a degenerative chain transfer mechanism or by a direct dissociation−recombination of the generated radical.[98] Visible light (405 nm) was used instead of UV in order to avoid possible irreversible photolysis of CTA under UV irradiation.[99] Given the weak absorption of CTA at 405 nm (n → π* electronic transition), a photo-initiator (TPO-L) was added to increase the kinetic of the photo-polymerization. In fact, preliminary tests of polymerization of HPMA from $DexCTA_{12}$ in water without TPO-L revealed slow monomers conversion (< 30%) within 8h of irradiation under 405 nm. The impact of the irradiation wavelength on the morphology of nanoobjects was not studied in the present paper.

The macromolecular RAFT agent based on dextran ($DexCTA_{12}$), containing CTA moieties (Fig. S1B†), was prepared using a novel pathway, more efficient and more reproducible, according to our recent paper. [11] Namely, hydroxyl functions of dextran were first partially oxidized with sodium periodate, leading to dextran containing aldehydes. Oxidized dextran was then reacted with ethylenediamine to produce aminated dextran. Finally, CTA groups were linked to the dextran backbone *via* amidation, giving the $DexCTA_{12}$ compound. The number of CTA groups per dextran chain (12 per chain) was calculated from ^{1}H NMR spectrum (Fig. S1B†) using the area ratio of the signals at 0.98 ppm (CH_3 relative to CTA) and from 4.2 ppm to 5 ppm (3 OHs and anomeric protons of dextran). The number-average molar mass ($\overline{M_n}$ = 37500 g mol^{-1}) and dispersity (Đ = 1.27) of $DexCTA_{12}$ were determined by SEC in DMSO/$NaNO_3$ (8.5 g L^{-1}) at 70 °C (Fig. S2†).

Effect of the self-assembly process: PISA vs traditional self-assembly processes.

In comparison to spheres, worm-like micelles (WLM) have various characteristics readily recognized by static/dynamic light scattering (typical form factor and $\rho = R_g/R_H$ ratio) and by transmission electron microscopy (morphology), making them ideal models to study the impact of the self-assembly process on the morphology of the obtained nanostructures. Thus, in the present work, WLM were first targeted by conducting PISA under specific experimental conditions, according to our previous investigation. [49]

Chain extension of the PHPMA grafts from $DexCTA_{12}$ was performed in water *via* photo-RAFT polymerization under visible irradiation (λ = 405 nm) at RT (Nano-1). A theoretical degree of polymerization of PHPMA grafts ($\overline{X_n}$ of each graft = 400) and a solids concentration (10% w/w solids) were targeted to favourite the formulation of WLM. [49] As evidenced from ^{1}H NMR analysis (Fig. S1C†), a high monomer conversion (> 99%) was achieved within 1 hour of irradiation, leading to Dex-g^{12}-$PHPMA_{400}$ glycopolymers, where 12 is the number-average of PHPMA grafts per dextran chain and 400 is the theoretical number-average degree of polymerization ($\overline{X_n}$) of each graft. In comparison to $DexCTA_{12}$, the SEC shows a shift of the Dex-g^{12}-$PHPMA_{400}$ chromatogram toward low elution volumes while maintaining a low dispersity (Đ = 1.21), indicating the uniform growth of grafts from the $DexCTA_{12}$ backbone (Fig. S2†).

The aqueous Nano-1 suspension was diluted, then characterised by light scattering (DLS/SLS), TEM and CryoEM without further purification. On the one hand, DLS analysis (table 1) reveals the formation of nanoobjects with a Z-average hydrodynamic radius (R_H) equal to 98 nm (PDI = 0.2), estimated according to Eq-2 and using a diffusion coefficient (D_0 = 2.18 10^{-12} m^2 s^{-1}), which is the slope of the linear dependence of relaxation rate (Γ) plotted *versus* q^2 (Fig. 2A). On the other hand, a Z-average radius of gyration (R_g) equal to 214 nm (table 1) was determined by analysing the SLS data (Fig. S4†) recorded from a series of Nano-1 suspensions with different concentrations ranging from 0.0625 g L^{-1} to 0.5 g L^{-1}, using the Zimm equation (Eq-3). As shown in table 1, the so-called ρ–ratio ($\rho = R_g/R_H$), which is an important indication of the morphology of scattering nanoobjects, is close to 2 ($\rho = 2.17$) and corresponds to a cylindrical morphology.[100] This represents a first confirmation of the formulation of WLM using photo-PISA at RT.[49]

The dependence of the normalized light scattering form factor of Nano-1, calculated from SLS data using Eq-6, on the scattering vector (q) is shown in Fig. 2B. The shape of the obtained curve constitutes an additional approach to study the morphology of nanoobjects. As shown in Fig. 2B, the curve of Nano-1 displays the slope q^{-1} scaling law over intermediate q wavevector range, characteristic of WLM, rather than q^{-2} or q^{-4} scaling laws characteristic of vesicles or spherical micelles, respectively.[101] In the literature, various model form factors were developed to fit the SLS data recorded for elongated nanoobjects. [102] The simplest model is that of monodisperse stiff cylinders (Eq-7) with length $L = R_g\sqrt{12}$. As shown in Fig. 2B, the normalized form factor of Nano-1 could be fitted using Eq-7 for intermediate length scales $4 < qL < 11$. However, a large deviation is observed at large length scales $qL > 11$, indicating that Nano-1 probably contains a mixture of morphologies.

$$\frac{P_1(\theta)}{P_1(\theta=20°)} \qquad \text{Eq-7}$$

With $P_1(\theta) = \frac{2}{qL}Si(qL) - 4\left(\frac{\sin(qL)}{qL}\right)^2$

and $Si(qL) = \int_0^{qL}\frac{\sin(qL)}{qL}d(qL)$ the sinus-integral-function.

Table 1. Summary of the characteristics and parameters used to fit the SLS data recorded at 20°C of the Dex-g[12]-PHPMA$_{400}$ -based nanostructures. WLM: worm-like micelle, S: sphere.

Entry	DLS/SLS				Fit parameters		Morphology
	R_H (nm)	R_g (nm)	ρ	PDI	Eq	Size (nm)	
Nano-1	98	214	2.17	0.2	Eq-7	L=741	WLM + S
					Eq-8	R=267	
					Eq-9	L=741, R=267	
Nano-2	88	75	0.85	0.11	Eq-8	R=98	S
Nano-5	47	40	0.85	0.06	Eq-8	R=50	S
Nano-6	88	68	0.77	0.10	Eq-8	R=88	S

A model form factor of spherical micelles [103] (Eq-8) was also tested in this study in order to establish the best fit for the SLS data. The parameters used are summarized in table 1. As expected, the theoretical expression of spherical micelles does not correspond to the experimental SLS data (Fig. 2B). It is important to note that the experimental values are located between curves of Eq-7 and Eq-8, meaning that Nano-1 obtained *via* the photo-PISA at RT may contain a mixture of cylindrical and spherical morphologies. This assumption was verified by using an empirical equation (Eq-9) that describes the average of the contribution of worm-like and spherical micelles, based on the statistical analysis determined from TEM analysis. As shown in Fig. 2B, Eq-9 fits the SLS data well over a wide range of length scales (qL).

$$\frac{P_2(\theta)}{P_2(\theta=20°)} \qquad \text{Eq-8}$$

With $P_2(\theta) = \frac{9}{(qR)^6}(\sin(qR) - qR\cos(qR))^2$

and R the radius of the sphere.

$$\frac{P_3(\theta)}{P_3(\theta=20°)} \qquad \text{Eq-9}$$

With $P_3(\theta) = 0.6 \times P_1(\theta) + 0.4 \times P_2(\theta)$

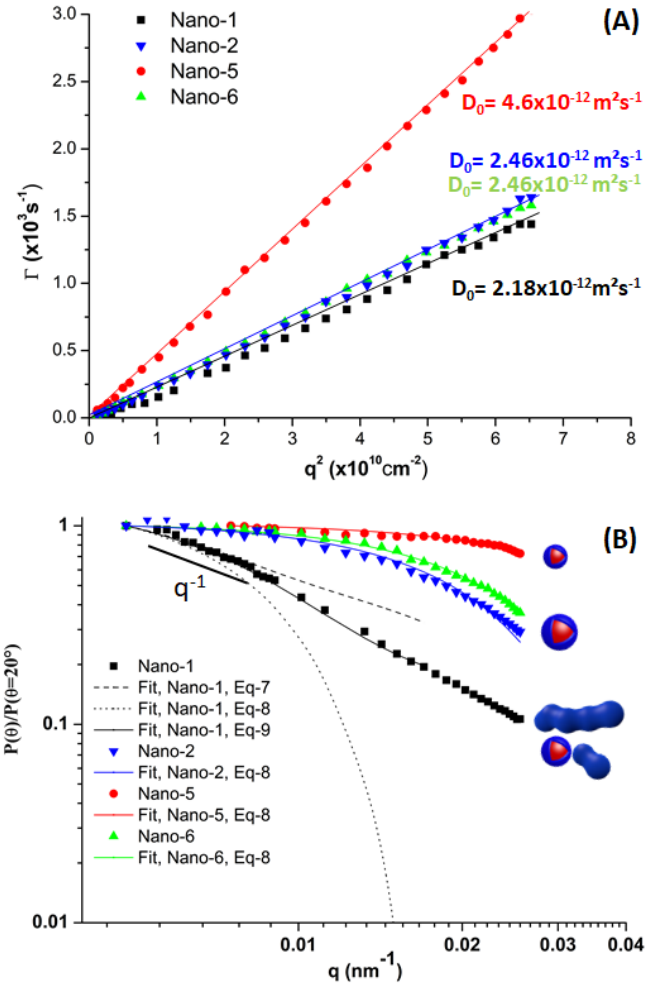

Fig.2 (A) q^2 dependence of the relaxation rate (Γ) obtained from DLS experiments at 20°C. (B) normalized form factors plotted *versus* q obtained from SLS measurements at 20°C for different nanostructure dispersions.

To further investigate the morphology of the nanostructures, the Nano-1 suspension was characterized by transmission electronic microscopy (TEM). Uranyl-acetate was added at very low concentrations to stain the nanostructures chemically. As shown in Fig. 3A and 3B, a mixed phase of spheres and oblate micelles with a significant proportion of WLM was observed. It is well-known that the preparation of samples for TEM characterization requires drying of the colloidal suspension, which can potentially induce damage and modification of the nanostructure morphology. Thus, one could assume that the observed WLM and oblate micelle morphologies were formed by the fusion of spherical micelles during the drying step. Cryogenic electron microscopy (CryoEM) is an elegant approach to minimize such damage, involving freezing of an aqueous sample in its hydrated state. A typical CryoEM image obtained for the Nano-1 suspension is shown in Fig. 3C, confirming the presence of worm-like micelles. Additional TEM and CryoEM images of Nano-1 are available in Fig. S5†. Note that a statistical study of the different TEM and CryoEM images reveals that Nano-1 suspension is mainly composed of WLM (> 60 %) (Fig. 3D), consistent with the results obtained by light scattering. These calculated proportions were used to establish empirical equation Eq-9.

In order to study the impact of the self-assembly process on the morphology of formed nanostructures, Nano-1 suspension was freeze-dried overnight to give a dried powder of Dex-g^{12}-PHPMA$_{400}$ glycopolymers. This powder was then dispersed in water using conventional assembly methods: nanoprecipitation (Nano-2), emulsion-solvent evaporation (Nano-3) and film-rehydration (Nano-4). For all methods, the glycopolymers were dispersed in the usual solvents used for each method (DMSO for Nano-2, CH_2Cl_2 or $CHCl_3$ for Nano-3, and THF or acetone for Nano-4) before addition of water. As shown in Fig. S6†, after elimination of the organic solvent, a homogeneous white dispersion was obtained for Nano-2 at 20 mg mL^{-1}, while white precipitates were formed for Nano-3 and Nano-4. The low solubility of the Dex-g^{12}-PHPMA$_{400}$ glycopolymers in CH_2Cl_2, $CHCl_3$, acetone and THF, prior adding water, could explain the formation of these precipitates instead of homogeneous suspensions. These early investigations demonstrate how it is difficult to find a common organic solvent for both parts of the glycopolymers and consequently to induce their self-assembly in water by emulsion-solvent evaporation and film-rehydration methods.

Various aqueous suspensions of Dex-g^{12}-PHPMA$_{400}$ -based nanoobjects were prepared by nanoprecipitation at different final concentrations (from 1 to 100 mg mL^{-1}) to study the impact of the glycopolymer concentration on the morphology of the resulting nanostructures. Unfortunately, white precipitates were obtained at higher concentrations (100 mg mL^{-1} and 50 mg mL^{-1}), whereas homogeneous suspensions were obtained for dilute dispersions (20 mg mL^{-1}, 10 mg mL^{-1} and 1 mg mL^{-1}). Light scattering analysis (table 1) of the Nano-2 suspension (20 mg mL^{-1}), prepared by nanoprecipitation, shows nanostructures with R_H = 88 nm, estimated according to Eq-2 and using $D_0 = 2.46\ 10^{-12}$ m² s^{-1} (Fig. 2A), and R_g = 75 nm determined by analysing the SLS data (Fig. S4†). A ρ-ratio (ρ = 0.85) close to 0.77 is obtained, suggesting the formation of spherical

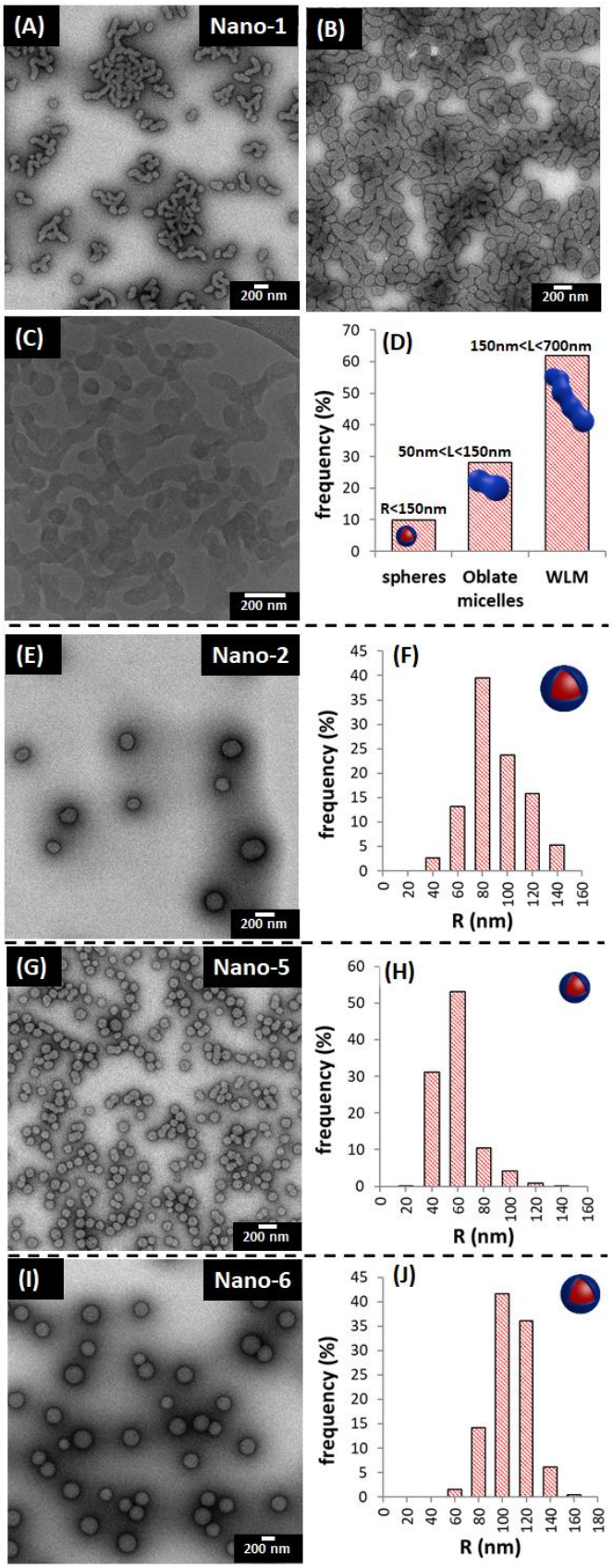

Fig.3 (A, B, E, G, I) TEM and (C) cryoTEM images of nanostructure suspensions based on Dex-g^{12}-PHPMA$_{400}$ obtained *via* different pathways (see Fig. 1). (D, F, H, J) statistical analysis made from 100 nanoobjects using ImageJ software.

micelles. By comparing the SLS data recorded for Nano-1 and Nano-2 (Fig. 2B), one can observe a significant difference between the normalized form factors of these two suspensions. Note that the SLS data of Nano-2 could be fitted using a spherical micelle form factor (Eq-8). These findings are consistent with the TEM characterization, where spherical micelles are observed (Fig. 3E, 3F). It should be noted that the other suspensions produced by nanoprecipitation at lower concentrations (10 mg mL^{-1} and 1 mg mL^{-1}) were characterized by DLS/SLS (data not shown) and by TEM. Spherical micelles were also observed as shown in Fig. S7†, suggesting that concentration does not have an impact on the nanostructure morphology.

Thus, our findings showed that the same glycopolymer (Dex-g^{12}-PHPMA$_{400}$) can form different order of morphologies in water depending on the assembly process used (WLM using PISA at RT, and spheres using nanoprecipitation), demonstrating how the morphology of glycopolymers-based nanoobjects depends strongly on the method of self-assembly used, in contrast to synthetic copolymers.[104]

Effect of the temperature during the PISA process.

Currently, apart from our previous work describing photo-PISA at RT,[49] all the other reports on the use of reactive polysaccharide derivatives as hydrophilic stabilizer for PISA were exclusively performed by thermal initiation.[73, 74] Surprisingly, if a large set of advanced morphologies was yielded in the former, only spherical morphology was reported in the latter. We hypothesised that temperature could have a strong effect on the morphology of the glyco-nanostructures produced by PISA. To the best of our knowledge, this challenging question has been never discussed in case of polysaccharidic steric stabilizers in PISA. However, it has been reported for some synthetic block copolymers. [58, 88]

Herein, to study the impact of temperature on the morphology of the glyco-nanostructures during the process of PISA, the aqueous photo-RAFT polymerization of HPMA from DexCTA$_{12}$ was carried out at 60 °C (Nano-5), using a similar experimental protocol of Nano-1 ($\overline{X_n}$ of each graft $= 400$ and 10% w/w solids). Fig. S8† shows the experimental setup used. As evidenced from ^{1}H NMR analysis (Fig. S1D†), a complete conversion of HPMA (> 99%) was achieved within 1 hour of irradiation. SEC analysis (Fig. S2†) shows uniform growing of the PHPMA grafts from DexCTA$_{12}$ backbone, leading to a glycopolymer (Nano-5) with macromolecular parameters ($\overline{M_n}$ = 134000 g mol^{-1}, Đ = 1.22) equivalent to the one estimated for Nano-1 ($\overline{M_n}$ = 135000 g mol^{-1}, Đ = 1.21). After one hour of irradiation at 60°C, a diluted sample was prepared and directly characterized by DLS at 60°C. The reaction medium was then cooled to RT, and a new diluted sample was prepared and characterized by DLS at 20°C. As shown in Fig. 4A, similar hydrodynamic radii were obtained by DLS performed at 60 °C (before cooling, R_H = 50 nm, PDI = 0.17) and at 20°C (after cooling, R_H = 47 nm, PDI = 0.06), suggesting the absence of any phase transition of nanoobjects from 60°C to RT. The slight difference in R_H is attributed to the relatively large PDI of Nano-5 at 60°C. It should be stressed that no visual changes were occurred during the cooling step. We assumed that the morphology formed at 60°C remained equivalent to the one at RT. Note that Nano-5 remained stable for several months at RT as evidenced by DLS results

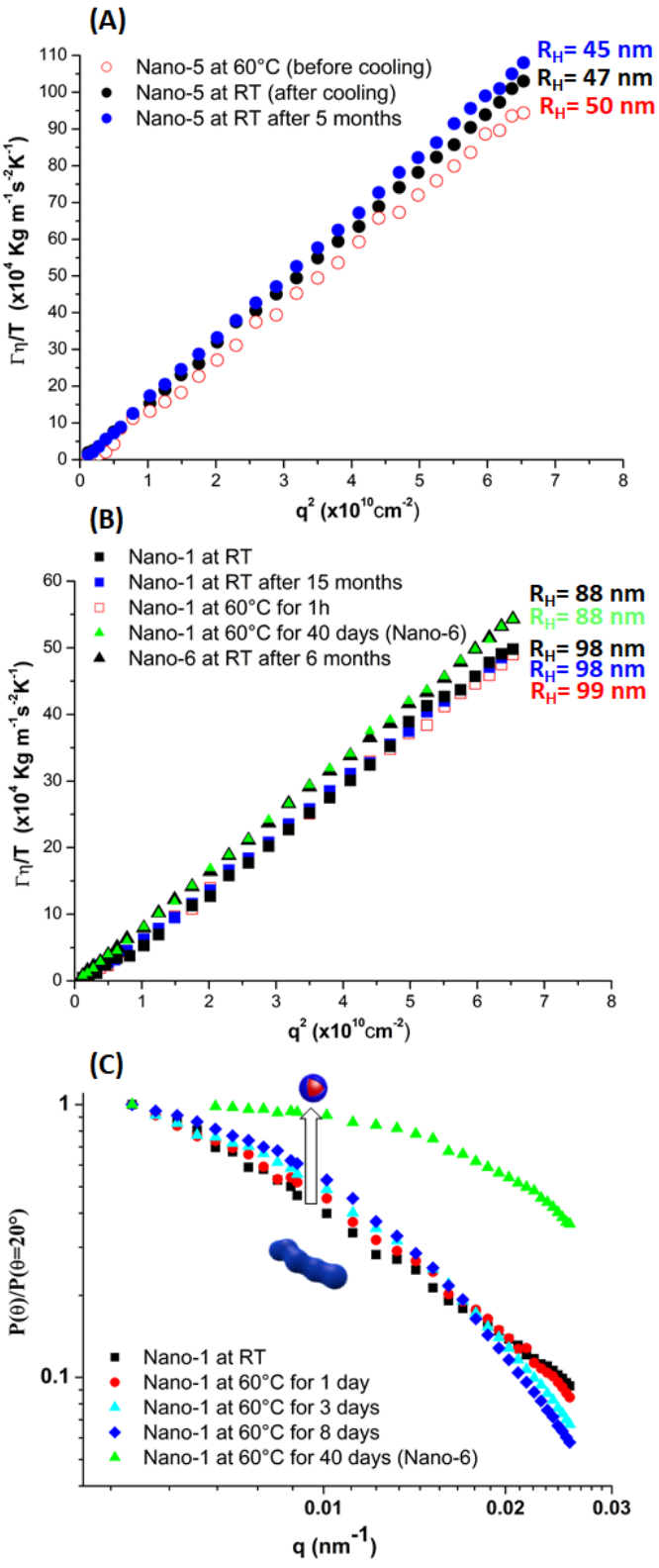

Fig. 4 Effect of temperature and storage period on the morphology of Nano-1, Nano-5 and Nano-6. (A) and (B) R_H was estimated from the slop ($k_B/3\pi R_H$) of q^2 dependence of ($\Gamma\eta_S/T$) recorded by DLS measurements (Eq-2) at 20°C (closed symbols) and at 60°C (open symbols). η is the viscosity of the water (η = 10^{-3} or 0.47×10^{-3} kg m^{-1} s^{-1} at 20°C or 60°C, respectively). (C) Evolution of the normalized form factors of Nano-1 at 60°C for different heating period.

(Fig. 4A), R_H = 45 nm, PDI = 0.09. A R_g = 40 nm was calculated at RT using a Zimm plot diagram (Fig. 4S†), leading to a ρ-ratio (ρ = 0.85) close to 0.77, which is characteristic of the spherical micelle morphology. Additionally, the SLS data of Nano-5, which are considerably different from those of Nano-1 (Fig. 2B), were fitted using the theoretical expression of spheres (Eq-8). TEM images (Fig. 3G and 3H) clearly reveal the spherical morphology formed during the photo-PISA at 60 °C. Additional TEM images are shown in Fig. S9†.

Our findings confirmed that performing PISA at different temperatures led to the formation of nanoobjects exhibiting different morphologies. More important, we demonstrated that increasing the temperature of polymerization in PISA (60°C) results in the formation of nanoobjects with lower order of morphology, i.e. spheres, instead of WLM formed by PISA at RT. This difference of morphology could be attributed to the change in the hydration state of the hydrophobic PHPMA grafts with temperature,[105] resulting in the variation of the hydrophobic / hydrophilic volume ratio (V_r) that drives the packing parameter (Fig. 5). PISA at RT produced WLM (Nano-1) because PHPMA grafts were more hydrated (increase of the hydrophobic PHPMA volume), which results in a larger V_r (higher packing parameter). In contrast, at 60°C, PHPMA grafts were less hydrated (more compact) leading to a lower V_r (smaller packing parameter) and thus resulting in the formation of lower-order morphology (spheres, Nano-5). Note that dextran does not undergo any conformational change at this range of temperature,[106] that would explain the difference of morphology observed by PISA at RT and 60°C.

It should be stressed that our findings are in contrast to the ones of Tan, Zhang and co-workers, who found, using macroCTAs based on poly(ethylene glycol)[58] and poly(glycerol monomethacrylate),[88] that increasing the temperature of photo-polymerization of HPMA led to higher order of assemblies (vesicles instead of spheres). Authors reported two explanations for their observations: i) the low aqueous solubility of HPMA at high temperature would induce an increase of local HPMA concentration within the micelles at early stage of polymerization (in comparison to RT), which favourites the formation of high order morphologies, [58] ii) the fusion of spheres at high temperature due to the increase of the PHPMA mobility [88] (T_g of HPMA in water =47 °C [27]). The unusual behaviour of our system can be explained as following. On the one hand, the higher surfactant properties of $DexCTA_{12}$, due to the presence of various CTA on dextran backbone, may confer uniform dispersion of HPMA in water at high temperature and thus avoids aggregation of monomers. On the other hand, the grafted architecture of Dex-g^{12}-$PHPMA_{400}$ glycopolymer may confer a higher stabilization of the nanostructures, avoiding mobility of the glycopolymers and thus the fusion of spheres into WLM.

Temperature induced phase transition.

One might legitimately wonder about the factor driving Dex-g^{12}-$PHPMA_{400}$ glycopoymers (Nano-1 and Nano-5) to *in fine* form different morphologies (WLM *vs* spheres) at the same temperature, i.e. RT. We assumed that the thermal history of nanoobjects could have a considerable effect on their morphologies. To verify this assumption, we decided to subject WLM previously prepared by photo-PISA at RT (Nano-1) to a thermal annealing, allowing Nano-1 to have a similar thermal history as Nano-5.

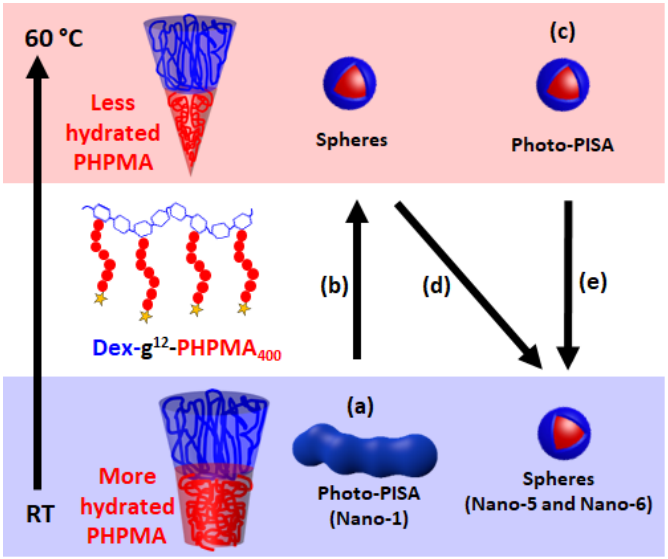

Fig. 5 Proposed mechanism explaining the effect of temperature on the morphological evolution of Dex-g^{12}-$PHPMA_{400}$-based nanoobjects at 10% w/w solids. (a) WLM prepared by photo-PISA at RT (Nano-1). (b) Irreversible transition of WLM to spheres by heating to 60°C. (c) Spherical micelles prepared by photo-PISA at 60°C. (d, e) Cooling of spheres dispersions prepared by routes b and c leading to spheres (Nano-6 and Nano-5, respectively).

The aqueous Nano-1 suspension (10 % w/w solids) was first heated to 60 °C for 1 hour. Immediately, a diluted sample was prepared and characterized by DLS at 60°C. Fig. 4B indicates that the R_H of Nano-1 remained unchanged after such heating (98 nm, PDI = 0.2 at 20°C instead of 99 nm, PDI = 0.12 at 60°C), suggesting that WLM remained stable at 60°C for one hour. These preliminary results indicate that no thermal transition was occurred under the experimental conditions of Nano-5. We assumed that the dehydration process of PHPMA would request a much longer time. Accordingly, we decided to increase the thermal annealing period.

As shown in Fig. 4C, WLM remained stable during the first incubation day at 60°C, as the shape of the normalized form factor was unchanged. However, after 8 days at 60°C, SLS data underwent a small deviation, then became completely different after 40 days of incubation at 60°C (Nano-6), indicating an evolution of the morphology. The normalized form factor of Nano-6 was well-fitted using the theoretical expression of spheres (Eq-8) as shown in Fig. 2B, confirming the evolution of the WLM (Nano-1) to spherical micelles (Nano-6). The ρ-ratio (ρ = R_g/R_H = 0.77) calculated (from the R_H = 88 nm and the R_g = 68 nm) for the Nano-6 suspension (table 1), and the TEM images (Fig. 3I, 3J and S10†) clearly reveal the presence of spherical micelles.

As summarized in Fig. 5, such thermal order-order transition (WLM to spheres) could be attributed to the decrease of the packing parameter at 60 °C caused by the weak hydrophobic nature of PHPMA-based core-forming nanoobjects (dehydration of PHPMA grafts by heating). It should be noted that such thermal transition is

irreversible, given that spheres formed at 60°C remained stable at RT for many months as evidenced by DLS results shown in Fig. 4B (R_H = 88 nm, PDI = 0.04). This could be attributed to the Dex-g^{12}-PHPMA$_{400}$ glycopolymers architecture (grafted), which may confer a higher stabilization of the nanostructures, avoiding the fusion of spheres into WLM. Analysis of Nano-1 suspension stored at RT in dark for 15 months (Fig. 4B) showed that WLM remained stable at RT (R_H = 98 nm, PDI = 0.12). This finding constitutes an additional proof that the WLM to spheres transition is induced by a thermal process rather than an aging phenomenon.

In the literature, inter-morphology thermal transitions have been previously reported for various PHPMA-based core-forming nanoobjects. [105, 107-111] Armes and co-workers reported reversible phase transformation between 4°C and 50°C for nanoobjects prepared by PISA using poly(ethylene glycol), [107] poly(glycerol monomethacrylate),[105, 108] and poly(N-(2-hydroxypropyl) methacrylamide) [110] as hydrophilic macroCTAs. Tan, Zhang and co-workers [112] observed irreversible transformation of WLM to spheres when cooling from RT to 4°C. Recently, Delaittre and co-workers [111] observed reversible phase transitions between 4°C and 40°C for poly(2-oxazoline)-b-PHPMA-based nanoobjects at high concentration, and an irreversible transition at low concentration (only vesicles to WLM to spheres were possible by cooling) due to the unfavourable fusion of spheres or WLM in diluted medium. [111] Note that our observations are again in contrast to those reported by such research groups, who found that heating aqueous suspensions of nanoobjects induced an increase of the morphology order, i.e. WLM to vesicles. Authors [110] ascribed this phenomenon to the surface dehydration of the PHPMA segments (closest to the hydrophilic block and previously preferentially hydrated at low temperature), which causes a reduction of the effective hydrophilic block size, resulting in higher V_r (higher packing parameter). In our case, we assume that the unusual behaviour of Dex-g^{12}-PHPMA$_{400}$ glycopolymers at high temperature is attributed to an uniform dehydration of the PHPMA, which causes a reduction of the volume of the PHPMA grafts, resulting in a smaller V_r and thus in the formation of lower order morphology.

Conclusion

In summary, the effect of the experimental conditions, used to induce the self-assembly of amphiphilic glycopolymers (AGPs) in water, on the produced nanoobjects morphology was highlighted using advanced characterization techniques, including static/dynamic light scattering and TEM/CryoEM analysis. A model amphiphilic grafted glycopolymer (Dex-g^{12}-PHPMA$_{400}$) based on dextran as hydrophilic polysaccharide backbone and PHPMA as hydrophobic grafts was investigated.

On the one hand, we demonstrated that the self-assembly of glycopolymers is sensitive to the process used. Formation of glyco-nanostructures using photo-PISA at RT led to a mixed phase of spheres with a major population of WLM, whereas the nanoprecipitation method, which is one of the most-used conventional self-assembly techniques, led only to spherical micelles. Additionally, we showed that the emulsion-solvent evaporation and film-rehydration techniques using usual solvents led to the precipitation of Dex-g^{12}-PHPMA$_{400}$ in water, indicating that these conventional assembly techniques are not suitable for such glycopolymers.

On the other hand, we demonstrated that the morphology of glyco-nanostructures was affected by temperature. Performing photo-PISA at 60 °C led to spheres instead of the WLM observed with photo-PISA at RT. Additionally, our findings revealed that WLM of Dex-g^{12}-PHPMA$_{400}$ underwent an unusual morphological transition to spheres upon incubation at 60 °C. We attribute such thermal behaviour to the weak hydrophobic nature of PHPMA-based core-forming nanoobjects, which changes with temperature, resulting in a shift of the hydrophobic/ hydrophilic volume ratio that drives the packing parameter.

We hope that this study contributes to the fundamental comprehension of the self-assembly of amphiphilic glycopolymers into nanostructures with advanced morphology, which is an important step in developing glyco-nanocarriers for drug delivery. We believe that the self-assembly of amphiphilic glycopolymers is far to be completely understood, many other parameters need to be deeply investigated, including nature of hydrophilic polysaccharide, number and size of grafts.

Conflicts of interest

There are no conflicts to declare.

Acknowledgements

The financial support from the French Agence Nationale de la Recherche (ANR JCJC, GlyNanEP N° 18-CE06-0002) is gratefully acknowledged. The authors acknowledge the CryoEM platform of I2BC, supported by iBiSA and by the French Infrastructure for Integrated Structural Biology (FRISBI) [ANR-10-INSB-05-05].

Notes and references

1. C. Schatz and S. Lecommandoux, *Macromol. Rapid Commun.*, 2010, **31**, 1664-1684.
2. Z. Liu, Y. Jiao, Y. Wang, C. Zhou and Z. Zhang, *Advanced Drug Delivery Reviews*, 2008, **60**, 1650-1662.
3. N. Goodarzi, R. Varshochian, G. Kamalinia, F. Atyabi and R. Dinarvand, *Carbohydrate Polymers*, 2013, **92**, 1280-1293.
4. A. Basu, K. R. Kunduru, E. Abtew and A. J. Domb, *Bioconjugate Chemistry*, 2015, **26**, 1396-1412.
5. T. G. Barclay, C. M. Day, N. Petrovsky and S. Garg, *Carbohydrate Polymers*, 2019, **221**, 94-112.
6. J. L. Six and K. Ferji, *Polym. Chem.*, 2019, **10**, 45-53.

7. L. I. Atanase, J. Desbrieres and G. Riess, *Progress in Polymer Science*, 2017, **73**, 32-60.
8. M. S. Verma and F. X. Gu, *Carbohydrate Polymers*, 2012, **87**, 2740-2744.
9. Z. Zhao, Z. Zhang, L. Chen, Y. Cao, C. He and X. Chen, *Langmuir*, 2013, **29**, 13072-13080.
10. Z. Zhang, X. Chen, X. Gao, X. Yao, L. Chen, C. He and X. Chen, *RSC Adv.*, 2015, **5**, 18593-18600.
11. D. Ikkene, A. A. Arteni, H. Song, H. Laroui, J. L. Six and K. Ferji, *Carbohydrate Polymers*, 2020, **234**, 115943.
12. H. L. Sun, B. N. Guo, X. Q. Li, R. Cheng, F. H. Meng, H. Y. Liu and Z. Y. Zhong, *Biomacromolecules*, 2010, **11**, 848-854.
13. A. Peyret, J. F. Trant, C. V. Bonduelle, K. Ferji, N. Jain, S. Lecommandoux and E. R. Gillies, *Polym. Chem.*, 2015, **6**, 7902-7912.
14. M. El Founi, S. M. A. Soliman, R. Vanderesse, S. Acherar, E. Guedon, I. Chevalot, J. Babin and J. L. Six, *J. Colloid Interface Sci.*, 2018, **514**, 289-298.
15. M. Lee, Y. W. Cho, J. H. Park, H. S. Chung, S. Y. Jeong, K. W. Choi, D. H. Moon, S. Y. Kim, I. S. Kim and I. C. Kwon, *Colloid Polym. Sci.*, 2006, **284**, 506-512.
16. T. Ouchi, T. Saito, T. Kontani and Y. Ohya, *Macromol. Biosci.*, 2004, **4**, 458-463.
17. C. Nouvel, J. Raynaud, E. Marie, E. Dellacherie, J. L. Six and A. Durand, *J. Colloid Interface Sci.*, 2009, **330**, 337-343.
18. M. Rajan and V. Raj, *Carbohydrate Polymers*, 2013, **98**, 951-958.
19. T. C. dos Santos, N. Rescignano, L. Boff, F. H. Reginatto, C. M. O. Simoes, A. M. de Campos and C. U. Mijangos, *Carbohydrate Polymers*, 2017, **173**, 638-644.
20. A. Roy, M. A. M. Valderrama, V. Daujat, K. Ferji, M. Leonard, A. Durand, J. Babin and J. L. Six, *Journal of Materials Chemistry B*, 2018, **6**, 5130-5143.
21. K. S. Joshy, S. M. Alex, S. Snigdha, N. Kalarikkal, L. A. Pothen and S. Thomas, *Int. J. Biol. Macromol.*, 2018, **107**, 929-937.
22. S. M. A. Soliman, M. El Founi, R. Vanderesse, S. Acherar, K. Ferji, J. Babin and J.-L. Six, *Colloids and Surfaces B: Biointerfaces*, 2019, **182**, 110393.
23. K. Ferji, C. Nouvel, J. Babin, M.-H. Li, C. Gaillard, E. Nicol, C. Chassenieux and J.-L. Six, *ACS Macro Lett.*, 2015, **4**, 1119-1122.
24. C. Schatz, S. Louguet, J.-F. Le Meins and S. Lecommandoux, *Angewandte Chemie International Edition*, 2009, **48**, 2572-2575.
25. G. Delaittre, J. Nicolas, C. Lefay, M. Save and B. Charleux, *Chem. Commun.*, 2005, 614-616.
26. G. Delaittre, C. Dire, J. Rieger, J.-L. Putaux and B. Charleux, *Chem. Commun.*, 2009, 2887-2889.
27. A. Blanazs, J. Madsen, G. Battaglia, A. J. Ryan and S. P. Armes, *J. Am. Chem. Soc.*, 2011, **133**, 16581-16587.
28. S. L. Canning, G. N. Smith and S. P. Armes, *Macromolecules*, 2016, **49**, 1985-2001.
29. B. Charleux, G. Delaittre, J. Rieger and F. D'Agosto, *Macromolecules*, 2012, **45**, 6753-6765.
30. J. Rieger, *Macromol. Rapid Commun.*, 2015, **36**, 1458-1471.
31. C. A. Figg, A. Simula, K. A. Gebre, B. S. Tucker, D. M. Haddleton and B. S. Sumerlin, *Chem. Sci.*, 2015, **6**, 1230-1236.
32. E. T. Garrett, Y. Pei and A. B. Lowe, *Polym. Chem.*, 2016, **7**, 297-301.
33. S. Y. Khor, J. F. Quinn, M. R. Whittaker, N. P. Truong and T. P. Davis, *Macromol. Rapid Commun.*, 2019, **40**, 22.
34. D. Le, D. Keller and G. Delaittre, *Macromol. Rapid Commun.*, 2019, **40**, 21.
35. X. Wang and Z. S. An, *Macromol. Rapid Commun.*, 2019, **40**, 14.
36. N. J. W. Penfold, J. Yeow, C. Boyer and S. P. Armes, *ACS Macro Lett.*, 2019, **8**, 1029-1054.
37. S. Varlas, J. C. Foster and R. K. O'Reilly, *Chem. Commun.*, 2019, **55**, 9066-9071.
38. W. J. Zhang, C. Y. Hong and C. Y. Pan, *Macromol. Rapid Commun.*, 2019, **40**.
39. F. D'Agosto, J. Rieger and M. Lansalot, *Angew. Chem.-Int. Edit.*, 26.
40. J. Yeow and C. Boyer, *Advanced Science*, 2017, **4**, 1700137.
41. G. Delaittre and B. Charleux, *Macromolecules*, 2008, **41**, 2361-2367.
42. M. J. Derry, L. A. Fielding and S. P. Armes, *Polym. Chem.*, 2015, **6**, 3054-3062.
43. Z. L. Ding, C. Q. Gao, S. Wang, H. Liu and W. Q. Zhang, *Polym. Chem.*, 2015, **6**, 8003-8011.
44. Z. An, Q. Shi, W. Tang, C.-K. Tsung, C. J. Hawker and G. D. Stucky, *J. Am. Chem. Soc.*, 2007, **129**, 14493-14499.
45. Y. Li and S. P. Armes, *Angewandte Chemie International Edition*, 2010, **49**, 4042-4046.

46. E. R. Jones, O. O. Mykhaylyk, M. Semsarilar, M. Boerakker, P. Wyman and S. P. Armes, *Macromolecules*, 2016, **49**, 172-181.
47. J. Lesagedelahaye, X. Zhang, I. Chaduc, F. Brunel, M. Lansalot and F. D'Agosto, *Angewandte Chemie - International Edition*, 2016, **55**, 3739-3743.
48. M. Guerre, M. Semsarilar, F. Godiard, B. Améduri and V. Ladmiral, *Polym. Chem.*, 2017, **8**, 1477-1487.
49. K. Ferji, P. Venturini, F. Cleymand, C. Chassenieux and J.-L. Six, *Polym. Chem.*, 2018, **9**, 2868-2872.
50. S. Piogé, T. N. Tran, T. G. McKenzie, S. Pascual, M. Ashokkumar, L. Fontaine and G. Qiao, *Macromolecules*, 2018, **51**, 8862-8869.
51. F. H. Sobotta, F. Hausig, D. O. Harz, S. Hoeppener, U. S. Schubert and J. C. Brendel, *Polym. Chem.*, 2018, **9**, 1593-1602.
52. P. Gurnani, C. P. Bray, R. A. E. Richardson, R. Peltier and S. Perrier, *Macromol. Rapid Commun.*, 2019, **40**.
53. X. Dai, L. Yu, Y. Zhang, L. Zhang and J. Tan, *Macromolecules*, 2019, **52**, 7468-7476.
54. G. Mellot, J. M. Guigner, L. Bouteiller, F. Stoffelbach and J. Rieger, *Angewandte Chemie - International Edition*, 2019, **58**, 3173-3177.
55. N. Busatto, J. L. Keddie and P. J. Roth, *Polym. Chem.*, 2020, **11**, 704-711.
56. S. Xu, T. Zhang, R. P. Kuchel, J. Yeow and C. Boyer, *Macromol. Rapid Commun.*, 2020, **41**.
57. J. Yeow, J. T. Xu and C. Boyer, *ACS Macro Lett.*, 2015, **4**, 984-990.
58. J. B. Tan, H. Sun, M. G. Yu, B. S. Sumerlin and L. Zhang, *ACS Macro Lett.*, 2015, **4**, 1249-1253.
59. G. Wang, Z. Wang, B. Lee, R. Yuan, Z. Lu, J. Yan, X. Pan, Y. Song, M. R. Bockstaller and K. Matyjaszewski, *Polymer*, 2017, **129**, 57-67.
60. K. Wang, Y. X. Wang and W. Q. Zhang, *Polym. Chem.*, 2017, **8**, 6407-6415.
61. B. Shi, H. Zhang, Y. Liu, J. Wang, P. Zhou, M. Cao and G. Wang, *Macromol. Rapid Commun.*, 2019, **40**, 1900547.
62. D. Le, M. Dilger, V. Pertici, S. Diabaté, D. Gigmes, C. Weiss and G. Delaittre, *Angewandte Chemie International Edition*, 2019, **58**, 4725-4731.
63. O. L. Torres-Rocha, X. Wu, C. Zhu, C. M. Crudden and M. F. Cunningham, *Macromol. Rapid Commun.*, 2019, **40**, 1800326.
64. J. C. Foster, S. Varlas, L. D. Blackman, L. A. Arkinstall and R. K. O'Reilly, *Angewandte Chemie International Edition*, 2018, **57**, 10672-10676.
65. D. B. Wright, M. A. Touve, L. Adamiak and N. C. Gianneschi, *ACS Macro Lett.*, 2017, **6**, 925-929.
66. J. Jiang, X. Zhang, Z. Fan and J. Du, *ACS Macro Lett.*, 2019, **8**, 1216-1221.
67. C. Grazon, P. Salas-Ambrosio, E. Ibarboure, A. Buol, E. Garanger, M. W. Grinstaff, S. Lecommandoux and C. Bonduelle, *Angewandte Chemie International Edition*, 2020, **59**, 622-626.
68. D. Cordella, F. Ouhib, A. Aqil, T. Defize, C. Jerome, A. Serghei, E. Drockenmuller, K. Aissou, D. Taton and C. Detrembleur, *ACS Macro Lett.*, 2017, **6**, 121-126.
69. D. Cordella, A. Debuigne, C. Jerome, Z. Kochovski, D. Taton and C. Detrembleur, *Macromol. Rapid Commun.*, 2016, **37**, 1181-1187.
70. C. E. Boott, J. Gwyther, R. L. Harniman, D. W. Hayward and I. Manners, *Nature Chemistry*, 2017, **9**, 785-792.
71. A. M. Oliver, J. Gwyther, C. E. Boott, S. Davis, S. Pearce and I. Manners, *J. Am. Chem. Soc.*, 2018, **140**, 18104-18114.
72. J. Bernard, M. Save, B. Arathoon and B. Charleux, *J. Polym. Sci. Pol. Chem.*, 2008, **46**, 2845-2857.
73. V. Kapishon, R. A. Whitney, P. Champagne, M. F. Cunningham and R. J. Neufeld, *Biomacromolecules*, 2015, **16**, 2040-2048.
74. F. L. Hatton, M. Ruda, M. Lansalot, F. D'Agosto, E. Malmström and A. Carlmark, *Biomacromolecules*, 2016, **17**, 1414-1424.
75. R. A. Olson, A. B. Korpusik and B. S. Sumerlin, *Chem. Sci.*, 2020.
76. N. Corrigan, J. Yeow, P. Judzewitsch, J. Xu and C. Boyer, *Angewandte Chemie International Edition*, 2019, **58**, 5170-5189.
77. S. Perrier, *Macromolecules*, 2017, **50**, 7433-7447.
78. M. Chen, M. J. Zhong and J. A. Johnson, *Chemical Reviews*, 2016, **116**, 10167-10211.
79. P. Xiao, J. Zhang, F. Dumur, M. A. Tehfe, F. Morlet-Savary, B. Graff, D. Gigmes, J. P. Fouassier and J. Lalevee, *Progress in Polymer Science*, 2015, **41**, 32-66.
80. A. Anastasaki, V. Nikolaou, Q. Zhang, J. Burns, S. R. Samanta, C. Waldron, A. J. Haddleton, R.

McHale, D. Fox, V. Percec, P. Wilson and D. M. Haddleton, *J. Am. Chem. Soc.*, 2014, **136**, 1141-1149.
81. N. J. Treat, B. P. Fors, J. W. Kramer, M. Christianson, C. Y. Chiu, J. R. de Alaniz and C. J. Hawker, *ACS Macro Lett.*, 2014, **3**, 580-584.
82. D. Konkolewicz, K. Schroder, J. Buback, S. Bernhard and K. Matyjaszewski, *ACS Macro Lett.*, 2012, **1**, 1219-1223.
83. Y. Guillaneuf, D. Bertin, D. Gigmes, D. L. Versace, J. Lalevee and J. P. Fouassier, *Macromolecules*, 2010, **43**, 2204-2212.
84. E. Yoshida, *Soft Matter*, 2019, **15**, 9849-9857.
85. T. G. McKenzie, Q. Fu, M. Uchiyama, K. Satoh, J. Xu, C. Boyer, M. Kamigaito and G. G. Qiao, *Advanced Science*, 2016, **3**, 1500394.
86. L. Lu, H. J. Zhang, N. F. Yang and Y. L. Cai, *Macromolecules*, 2006, **39**, 3770-3776.
87. L. D. Blackman, K. E. B. Doncom, M. I. Gibson and R. K. O'Reilly, *Polym. Chem.*, 2017, **8**, 2860-2871.
88. J. B. Tan, D. D. Liu, Y. H. Bai, C. D. Huang, X. L. Li, J. He, Q. Xu, X. C. Zhang and L. Zhang, *Polym. Chem.*, 2017, **8**, 1315-1327.
89. V. Tkachenko, C. Matei Ghimbeu, C. Vaulot, L. Vidal, J. Poly and A. Chemtob, *Polym. Chem.*, 2019, **10**, 2316-2326.
90. P. Lertturongchai, M. I. A. Ibrahim, A. Durand, P. Sunintaboon and K. Ferji, *Macromol. Rapid Commun.*, 2020, **41**, 2000058.
91. J. B. Tan, Y. H. Bai, X. C. Zhang, C. D. Huang, D. D. Liu and L. Zhang, *Macromol. Rapid Commun.*, 2016, **37**, 1434-1440.
92. J. Tan, X. Li, R. Zeng, D. Liu, Q. Xu, J. He, Y. Zhang, X. Dai, L. Yu, Z. Zeng and L. Zhang, *ACS Macro Lett.*, 2018, **7**, 255-262.
93. Z. Liu, G. Zhang, W. Lu, Y. Huang, J. Zhang and T. Chen, *Polym. Chem.*, 2015, **6**, 6129-6132.
94. J. Yeow, O. R. Sugita and C. Boyer, *ACS Macro Lett.*, 2016, **5**, 558-564.
95. S. Shanmugam, J. T. Xu and C. Boyer, *J. Am. Chem. Soc.*, 2015, **137**, 9174-9185.
96. B. Nomeir, O. Fabre and K. Ferji, *Macromolecules*, 2019, **52**, 6898-6903.
97. J. Yeow, S. Shanmugam, N. Corrigan, R. P. Kuchel, J. T. Xu and C. Boyer, *Macromolecules*, 2016, **49**, 7277-7285.
98. T. G. McKenzie, Q. Fu, E. H. H. Wong, D. E. Dunstan and G. G. Qiao, *Macromolecules*, 2015, **48**, 3864-3872.
99. T. G. McKenzie, L. P. D. Costa, Q. Fu, D. E. Dunstan and G. G. Qiao, *Polym. Chem.*, 2016, **7**, 4246-4253.
100. C. A. Dreiss, *Soft Matter*, 2007, **3**, 956-970.
101. T. P. T. Dao, A. Brulet, F. Fernandes, M. Er-Rafik, K. Ferji, R. Schweins, J. P. Chapel, F. M. Schmutz, M. Prieto, O. Sandre and J. F. Le Meins, *Langmuir*, 2017, **33**, 1705-1715.
102. T. Fuetterer, A. Nordskog, T. Hellweg, G. H. Findenegg, S. Foerster and C. D. Dewhurst, *Physical Review E*, 2004, **70**, 041408.
103. L. Rayleigh, *Proceedings of the Royal Society of London. Series A, Containing Papers of a Mathematical and Physical Character*, 1910, **84**, 25-46.
104. M. K. Kocik, O. O. Mykhaylyk and S. P. Armes, *Soft Matter*, 2014, **10**, 3984-3992.
105. A. Blanazs, R. Verber, O. O. Mykhaylyk, A. J. Ryan, J. Z. Heath, C. W. I. Douglas and S. P. Armes, *J. Am. Chem. Soc.*, 2012, **134**, 9741-9748.
106. A. Durand and E. Dellacherie, *Biomacromolecules*, 2006, **7**, 958-964.
107. N. J. Warren, O. O. Mykhaylyk, D. Mahmood, A. J. Ryan and S. P. Armes, *J. Am. Chem. Soc.*, 2014, **136**, 1023-1033.
108. N. J. Warren, M. J. Derry, O. O. Mykhaylyk, J. R. Lovett, L. P. D. Ratcliffe, V. Ladmiral, A. Blanazs, L. A. Fielding and S. P. Armes, *Macromolecules*, 2018, **51**, 8357-8371.
109. S. J. Byard, C. T. O'Brien, M. J. Derry, M. Williams, O. O. Mykhaylyk, A. Blanazs and S. P. Armes, *Chem. Sci.*, 2020, **11**, 396-402.
110. L. P. D. Ratcliffe, M. J. Derry, A. Ianiro, R. Tuinier and S. P. Armes, *Angewandte Chemie - International Edition*, 2019, **58**, 18964-18970.
111. D. Le, F. Wagner, M. Takamiya, I. L. Hsiao, G. Gil Alvaradejo, U. Strähle, C. Weiss and G. Delaittre, *Chem. Commun.*, 2019, **55**, 3741-3744.
112. J. B. Tan, Y. H. Bai, X. C. Zhang and L. Zhang, *Polym. Chem.*, 2016, **7**, 2372-2380.